phys. stat. sol. (a) **205**, No. 3, 461–474 (2008) / **DOI** 10.1002/pssa.200723411

physica status solidi a
www.pss-a.com
applications and materials science

Feature Article

In-situ X-ray scattering studies of OFET interfaces

Alexander Gerlach[1], Stefan Sellner[1, 2, 3], Stefan Kowarik[1], and Frank Schreiber[*, 1]

[1] Institut für Angewandte Physik, Universität Tübingen, Auf der Morgenstelle 10, 72076 Tübingen, Germany
[2] Max-Planck-Institut für Metallforschung, Heisenbergstraße 3, 70569 Stuttgart, Germany
[3] School of Engineering and Applied Sciences, Harvard University, 29 Oxford Street, Cambridge, MA-02138, USA

Received 1 September 2007, revised 19 November 2007, accepted 4 December 2007
Published online 25 February 2008

PACS 61.05.cm, 68.35.Ct, 72.80.Le, 81.07.Pr

[*] Corresponding author: e-mail frank.schreiber@uni-tuebingen.de, Phone: +49-7071-2978663, Fax: +49-7071-295110

We review recent work in the field of organic thin films and organic-inorganic interfaces which is relevant for device applications and particularly organic field effect transistors (OFETs). Focussing on the structural properties of these systems we discuss results obtained mostly through X-ray scattering techniques. We address the growth behaviour and interface formation of organic thin films including roughness evolution and crystal structure. In particular, we review real-time studies of pentacene, diindenoperylene, and PTCDA deposition on different subtrates which illustrate their specific growth kinetics. Covering different thickness regimes we show how the molecular orientation depends on the substrate and the growth conditions. Finally, we address the structural properties of organic heterostructures, i.e. metal and insulator films on organics, demonstrating how to assess and control interdiffusion and thermal stability of the capping layers.

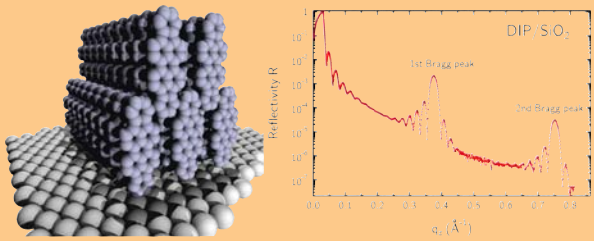

Schematic of stacked diindenoperylene molecules and corresponding X-ray reflectivity data.

1 Introduction The advent of organic, molecular semiconductors for electronic and optoelectronic applications has opened new possibilities for manufacturing of devices with large area, flexible structure, low temperature processing and low cost [1–4]. All these devices crucially depend on the definition of interfaces between functional materials and the structural (crystalline) order within the organic semiconductor itself [5]. While for the growth of inorganic materials a certain level of understanding has been reached, the growth of organic molecules poses a range of new challenges due to the weaker van-der-Waals binding forces within this 'soft matter' and new degrees of freedom impact growth, such as molecular orientation and conformation [6, 7]. Here we review our work on controlling the growth of organic semiconductor as well as the interface formation between inorganic insulators and metals with organic thin films. As is obvious from a generic sketch of an organic field effect transistor (OFET), interfaces play a crucial role in its performance: the metal/organic semiconductor interface determines charge carrier injection, while the interface between gate insulator/organic semiconductor is crucial in the formation – or interruption – of a conducting channel. This structure-function relation is also illustrated in several other contributions to this special issue. Apart from the use as gate dielectric, insulators may also be used to encapsulate devices, which is crucial for device operation and preventing device breakdown as many organic semiconductors degrade by exposure to oxygen or humidity. According to these challenges in controlling growth and manufacturing this review covers the following systems: (1) thin films of organic semiconductors on different substrates and (2) organic heterostructures, i.e. metal contacts on top of organics and aluminium oxide capping layers which are the basic build-

ing blocks of OFETs. It does not cover the organic/organic interface which is relevant for bipolar devices such as solar cells or bipolar transistors, and also modification of growth by self-assembled monolayers will not be discussed here.

In the growth studies presented below emphasis is put on X-ray scattering techniques, which are well suited to measure the properties of organic thin films as they are non-invasive, i.e. they can be used for *in-situ* studies in an ultra-high vacuum environment and they can be performed in real-time during organic molecular beam deposition (OMBD). We make extensive use of the capability of X-ray experiments to follow changes in sample structure, which allows one to study the growth mode during thin film deposition, but also the breakdown of encapsulated thin films can be directly measured. Also, *in-situ* studies offer the advantage that post-growth sample changes such as oxidation or de-wetting do not obscure the results. From the X-ray data one can extract parameters such as film thickness and roughness, fractional coverage of individual layers, crystal structure, mosaicity, bonding distances between substrate and molecules, island sizes and correlation lengths as will be shown below. Of great importance for understanding the organic/inorganic interface is the ability of X-rays to penetrate into the sample and thereby provide access to microscopic properties also of buried interfaces.

This review is organised as follows: After giving a short introduction to X-ray scattering for the investigation of thin films (Section 2), we address some aspects of growth physics which are relevant for organic materials (Section 3). Focusing on the molecules shown in Fig. 1 we then present three case studies of growth and interface formation for the systems pentacene on silicon oxide, diindenoperylene (DIP) on silicon oxide, and perylene-tetracarboxylicacid-dianhydride (PTCDA) on noble metals (Section 4). Increasing the complexity of the systems we finally cover structural properties of organic heterostructures, i.e. metal and insulator films on DIP (Section 5). These case studies are based mostly on our own work, but we provide numerous references to related studies in the literature.

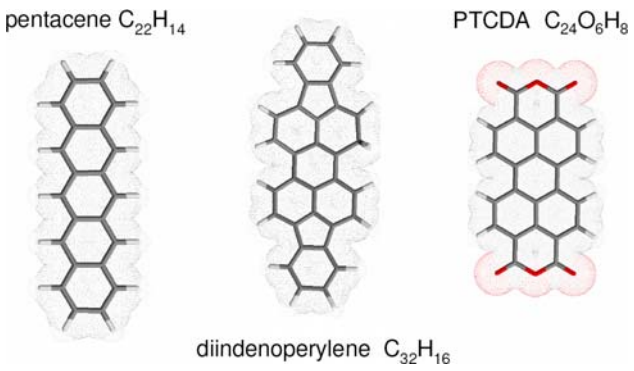

Figure 1 (online colour at: www.pss-a.com) Conjugated molecules of pentacene, diindenoperylene (DIP), and perylene-tetracarboxylicacid-dianhydride (PTCDA).

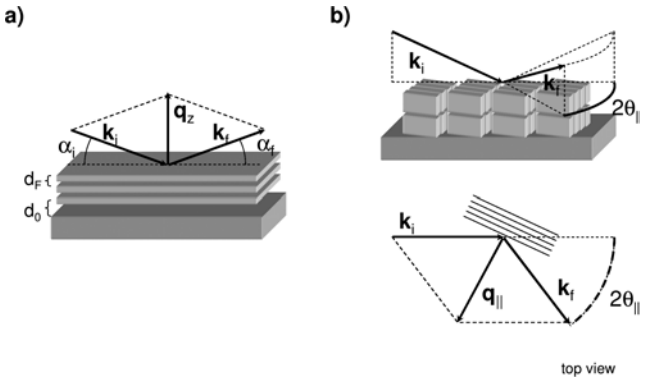

Figure 2 Scattering geometries with the corresponding initial and final wave vector $\boldsymbol{k}_i$ and $\boldsymbol{k}_f$. (a) Setup for specular X-ray reflectivity measurements which reveal the sample structure (roughness, lattice spacing) along the surface normal. (b) Setup for grazing incidence diffraction (GID), which measures lattice constants parallel to the sample surface. In both cases the initial and final wave vector $\boldsymbol{k}_i$ and $\boldsymbol{k}_f$ define the scattering plane.

2 X-ray scattering Various X-ray scattering techniques for the investigation of bulk properties are well established. Due to the increased availability of synchrotron light and advanced detector systems X-ray studies of low dimensional systems, interfaces, and thin films – even for organic materials with their low scattering cross section – have become feasible. According to the principal X-ray scattering geometries shown in Fig. 2 structural information can be derived both along the surface normal (out-of-plane) and parallel to the surface (in-plane). In the reciprocal space representation these measurements correspond to a momentum transfer along q_z and $q_{||}$, respectively. X-ray scattering data with high resolution and dynamic range taken in these geometries can be analysed quantitatively [8–11].

Since X-ray reflectivity (XRR) measurements on the specular path, i.e. with $q_{||} = 0$, probe the electron density along the surface normal, information about the film thickness D, surface and interface roughness σ, and the density ρ can be obtained [8]. With a layer model of the film the measured reflectivity curves can be analysed using either a kinematical approximation or the dynamical Parratt formalism [9]. Interference patterns with a periodicity of $2\pi/D$ in reciprocal space, so-called 'Kiessig fringes', which originate from the scattering at different interfaces (e.g., substrate-film and film-air), yield the parameters of the different layers. For a well-ordered film structure along the surface normal Bragg reflections observed at certain q_z-values give the spacing d_F of the individual layers shown in Fig. 2. For rough surfaces a significant part of the reflected intensity is scattered off-specular. This diffuse part contains information on the statistical properties of the surfaces and interfaces, such as the lateral correlation length ξ [10].

If the incident X-ray beam illuminates the surface at an angle smaller than the critical angle for total external reflection a so-called 'evanescent wave' is created, i.e. an

electric field with exponentially decaying amplitude inside the sample [11]. This transmitted wave, which parallel to the surface still has oscillating character, can give rise to Bragg reflections from periodic structures in the plane with a corresponding momentum transfer $q_{\|}$. Using this technique of 'grazing incidence diffraction' (GID), the in-plane structure can be studied (down to $z \approx 50$ Å). These two scattering geometries will be applied in the following to study the structural evolution during and after thin film deposition.

3 Growth physics Growth of crystalline thin films is a rich subject with many different facets and theoretical approaches [12–15]. Here we only address some important aspects which are relevant for organic thin film growth [16], particularly the interface formation in the first monolayer and the different growth modes of organic molecules (see Fig. 3).

3.1 Monolayer deposition It has been demonstrated that the first monolayer forms the crucial template for the growth of further molecular layers [16, 17], and the strength of the adsorbate-substrate interaction, the orientation of the molecules, their bonding distances to the topmost substrate layer determine to some extent the properties of the multilayer film. The bonding distance d_0 of the monolayer (Fig. 2) is one of the central quantities in this context and can be determined, e.g., by X-ray scans on the specular path [18]. More precise and chemically resolved structural information, however, can be obtained from X-ray standing wave (XSW) experiments [19]. As will be discussed below XSW measurements of various organic molecules on metal substrates [20–27] show that even for molecules in a lying-down orientation the bonding distance depends strongly on the substrate-adsorbate interaction. The exact knowledge of bonding distance and molecular conformation becomes particularly important in the light of recent reports [28], that the electronic structure of the metal/organic interface depends on adsorption geometry of the first molecular layer. The injection barriers for electrons (and holes) from the electrode into the organic layer, which affect the performance of the organic device, is thereby related to the monolayer structure.

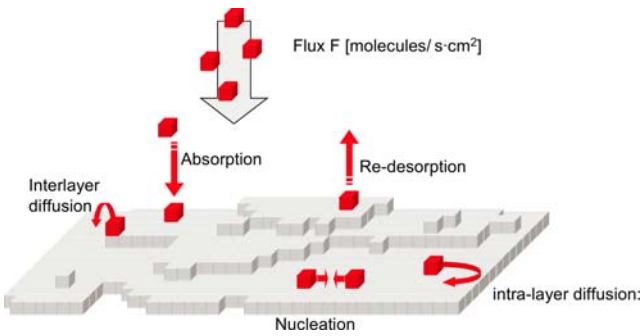

Figure 3 (online colour at: www.pss-a.com) Schematic of atomistic processes relevant for OMBD.

For growth on crystalline substrates, we also note that the strain induced by the lattice mismatch at the film-substrate interface is not only important in a crystallographic sense [29], but also influences the growth beyond the structure of the first monolayer. For example, it has been shown that DIP grown on NaCl single crystals exhibits herringbone type packing, but when DIP is grown on crystalline perylene thin films an unusual sandwich herringbone type packing is observed [30]. This suggests the possibility of controlling the stacking of epitaxial layers by careful selection of organic substrates beyond the first monolayer. For further details on organic epitaxy see the review by Hooks et al. [31].

3.2 Thin film growth and dynamic scaling For multilayer coverage one can distinguish three growth modes: island (Volmer–Weber), layer-plus-islands (Stranski–Krastanov), and layer-by-layer (Frank–van-der-Merwe) growth. Thermodynamic reasoning can be used to relate the surface energies $\gamma_{\text{substrate}}$, γ_{film}, and $\gamma_{\text{interface}}$ to these different growth scenarios. The details of the growth, however, usually also depend on the deposition rate and the temperature of the sample, In order to change the growth behaviour specific modification of the substrate surface energy $\gamma_{\text{substrate}}$ is often desirable. This can be achieved, for example, by functionalizing the substrate using self-assembled monolayers (SAMs) [32]. Several studies used alkanethiol SAMs on Au(111) to modify the growth of PTCDA films [33–35]. Similarly, SAMs have been used to modify the growth of pentacene thin films [36–39]. A more detailed discussion of this approach can be found in Ref. [32].

For a thorough description of a given growth scenario one might use specific growth models to quantify properties such as island size or film roughness and their evolution with film thickness. For island growth leading to roughening of the film surface rate equation models can be used [40]. In cases with little knowledge of atomic processes the roughness evolution can be more generally expressed in terms of growth exponents and dynamic scaling theories [41–43] which relate the growth mechanisms to a set of scaling exponents. Within this framework the film morphology can be described by three key parameters: the typical surface slope a, the correlation length ξ beyond which the heights at two points become uncorrelated, and the standard deviation of the film height σ (RMS roughness). These parameters scale with film thickness D according to

$$a \sim D^{\lambda}, \qquad \xi \sim D^{1/\tilde{z}}, \qquad \sigma \sim D^{\beta},$$

defining the steepening exponent λ, the dynamic exponent $\tilde{z}$, and the growth exponent β. Interestingly, both DIP on silicon oxide [44] as well as phthalocyanines [45] seem to display pronounced roughening, i.e. high β-values. Roughening parameters $\beta > 0.5$ indicate roughening faster than expected for random deposition in a 'hit-and-stick' model.

Such 'rapid roughening' has been measured for DIP/SiO_2 ($\beta = 0.748 \pm 0.05$) [44], H_2Pc/glass ($\beta = 1.02 \pm 0.08$), and plasma polymer ($\beta = 0.7 \pm 0.10$) [45], but the effect is also found in inorganic materials [46].

3.3 Growth of organic molecular materials While the general considerations above apply both to organic and inorganic materials, there are several specific challenges related to the growth of organic materials. These may arise from the commonly encountered polymorphism (simultaneous occurrence of different structural phases), the complex epitaxial relations (different unit cell sizes of substrate and adsorbate), or the heterogeneous material properties at the interface (interdiffusion, different thermal expansion of the organic thin film and the substrate).

Moreover, the growth itself may be complicated by the additional internal degrees of freedom (DOF) characteristic for organic molecules. The vibrational DOF can affect the interaction with the substrate and also the thermalization upon adsorption on the surface. Conformational DOF mean that the building block can change within the film, for example by bending to accommodate stress. Käfer et al. [7] found that the conformation of the organic semiconductor rubrene changes during growth, which may influence the film morphology [47]. Orientational DOF which are not included in conventional growth models can give rise to tilt domains and thereby an additional source of disorder, or may even entail the growth of competing 'lying down' and 'standing up' structures [6, 37] in the film as discussed below for the example of DIP.

The interaction between molecules and between molecules and non-metallic substrates is often dominated by weak van-der-Waals forces. It is important to emphasise that when integrated over all atoms within a molecule, the weak interaction energies add up and lead to substantial molecular binding energies. Nevertheless, the weaker interactions per atom lead to 'softer' materials and, for example, strain can be accommodated more easily. Due to the weaker interactions the thermal expansion coefficients (typically in the 10^{-4} 1/K range) are large when compared to inorganic materials, which possibly leads to higher thermally induced strain at film-substrate interfaces.

The size of the molecules and consequently the size of the unit cell is larger than that of inorganic materials. Therefore, the molecule-substrate interaction is averaged over a larger area with generally incommensurate (sub)structures. Due to this averaging the molecules experience a weaker specific interaction with the substrate. Also more translational and orientational domains for epitaxy on inorganic substrates are possible because of the different unit cell size. This introduces an additional source of disorder for organics.

4 Organic thin films Below we present three case studies for OMBD which demonstrate how X-ray scattering techniques can be used to derive not only precise structural information, but also details of the growth on different substrates.

4.1 Pentacene on silicon oxide Pentacene is attracting considerable attention as its charge transport properties are excellent [4, 48], and films of pentacene on silicon oxide are commonly used for thin film transistors in which the silicon oxide serves as gate dielectric.

Its thin film structure on silicon oxide as well as modified silicon surfaces has been studied extensively [51, 52]. Recently, the molecular arrangement within the unit cell has been solved using X-ray scattering [53, 54]. A dynamic-scaling analysis of the island distribution in submonolayer films shows that islands containing three or more molecules are stable [43, 55]. A modification of the hydrophobicity of the substrate has been shown to change the nucleation density of pentacene islands as well as the island size [38]. Under optimised conditions the island size in pentacene thin films can be as large as 0.1 mm [56]. In addition to varying substrate temperature and deposition rate, the kinetic energy of pentacene molecules has been varied in supersonic beam deposition [36, 57], providing an additional free parameter to influence the growth.

Using real-time techniques, the details of growth can be studied during deposition, yielding information about the dendritic island shape [56] as well as the coverage of individual layers [50, 58, 59]. From the X-ray reflectivity measurements shown in Fig. 4, not only the crystal structure can be determined from the positions of the Bragg reflections, but also the evolution of the film roughness can be extracted. It was shown by Mayer et al. [60] that a second pentacene phase [51, 52, 61] nucleates already in the first pentacene monolayer as could be determined from following the Bragg reflections corresponding to the two phases.

From the data in Fig. 4 as well as GID data [50], it can be seen that only the thin-film phase of pentacene [52] is growing for the conditions employed (out-of-plane lattice constant of $d_F = 15.6$ Å). Analysing not only the Bragg reflections, but also the evolution of the reflectivity between the Bragg reflections, we obtain additional information. Halfway between the Bragg reflections, i.e. $q_z = \pi/d_F$, at the so-called anti-Bragg point the interference of X-rays scattered from neighbouring layers interferes destructively, leading to an oscillating X-ray reflectivity when subsequent pentacene layers are filled. From these oscillations the number of pentacene monolayers that have been grown can be directly counted (oscillation period two monolayers). As can be seen from Fig. 4 the X-ray reflectivity shows modulations not only at the anti-Bragg condition, but also at all q-values other than the Bragg condition. These growth oscillations at different q-points correspond to the several Fourier components of the real-space structure. Therefore, it is advantageous to measure the reflectivity in a wide q-space region (0.25–0.8 $Å^{-1}$ in this case) to get a precise measurement of the real-space structure and the film roughness [62].

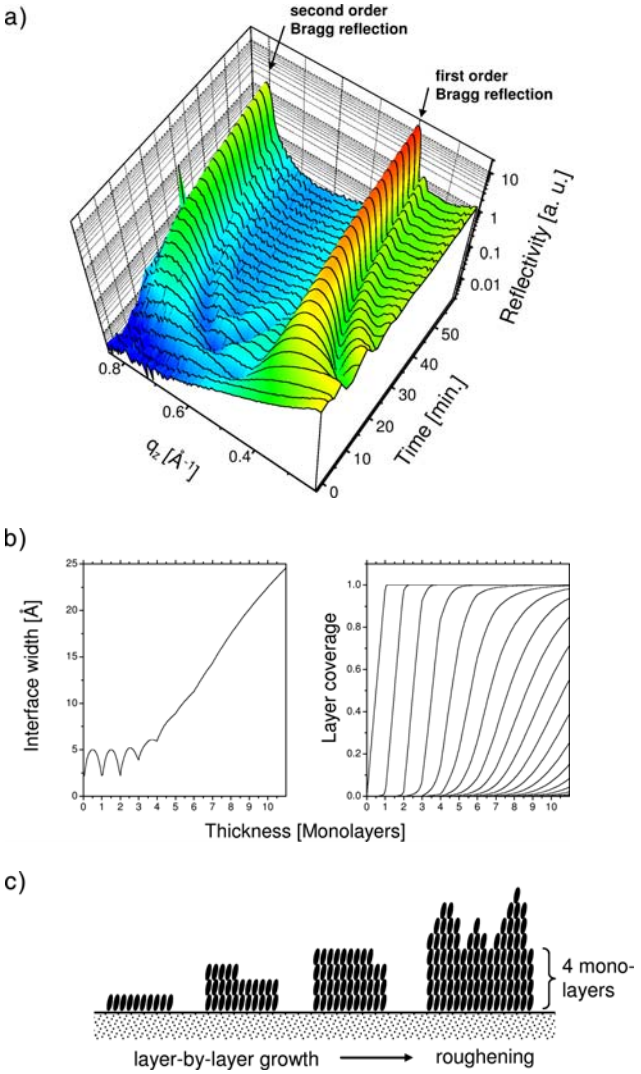

Figure 4 (online colour at: www.pss-a.com) (a) Real-time measurements of the X-ray reflectivity in a wide q-range during pentacene deposition on silicon oxide have been performed with energy dispersive data acquisition [49] (deposition rate 3.5 Å/min, substrate temperature 50 °C). Two peaks corresponding to the first and second order Bragg reflection of the pentacene thin film phase can be seen to grow with increasing deposition time (from Ref. [50] with permission). (b) Using a diffusive growth model and the kinematic approximation in X-ray scattering the interface roughness of the pentacene film and the coverage of individual layers during growth can be extracted from the data-set. (c) From the evolution of the surface roughness it can be seen that layer-by-layer growth persists for the first four monolayers before roughening sets in.

For pentacene, the roughness data show a clear change in growth mode after four monolayers. While the growth oscillations in the beginning indicate that pentacene grows in a layer-by-layer fashion (with an oscillating surface roughness), after four monolayers the roughness starts to increase. This is due to an incomplete filling of individual layers which results in a higher film roughness and a reduced electron density at the interface. A change of the growth mode from layer-by-layer growth to roughening has also been observed in Refs. [58, 59], where the interlayer transport of pentacene molecules could be quantified. While the exact nature of this transition is unknown, several factors may contribute such as decreased interlayer transport (increasing Schwoebel barrier), faster nucleation, and decreased diffusivity on top of islands.

4.2 DIP on silicon oxide Diindenoperylene (sometimes also referred to as periflanthene) is an organic semiconductor with both electron and hole conduction in single crystals, making this compound interesting for ambipolar electronics [63]. Thin film transistors with hole mobilities of up to 8×10^{-2} cm^2/Vs have been reported [48, 64], and recent experiments show that mobilities beyond 10^{-1} cm^2/Vs are feasible [65]. Further applications of DIP include usage for optical recording and in organic light emitting diodes [66, 67].

Growth of DIP molecules was studied in considerable detail [44, 68, 69]. When prepared under suitable conditions organic thin films of DIP deposited on silicon oxide exhibit high structural out-of-plane order [44]. The films form large flat terraces with a step height corresponding to the lattice spacing $d_F = 16.5$ Å as derived from the position of the DIP Bragg peak. On silicon oxide at high substrate temperature (≥100 °C), DIP grows in a mostly 'standing upright' orientation (NEXAFS measurements give a tilt angle of $83 \pm 5°$). The coherent thickness as determined from the Laue fringes around the first order Bragg reflection at $q_z = 0.38$ Å^{-1} corresponds almost to the total film thickness as determined from Kiessig oscillations [69]. This demonstrates that the DIP films are coherently ordered over the entire thickness. Rocking widths of about 0.01° and lower measured for DIP films confirm the high order/fiber texture of the films perpendicular to the sample surface. Within the surface plane the films are polycrystalline with an isotropic distribution of crystallite orientations on silicon oxide.

To study the temperature dependent growth dynamics and to establish the growth mode, the X-ray reflectivity in a q-range from the anti-Bragg condition to the Bragg point has been measured in real-time during DIP deposition (Fig. 5). For all three substrate temperatures studied the development of a strong Bragg reflection corresponding to standing upright molecules can be seen. Laue fringes develop and narrow with increasing film thickness next to the Bragg reflection. The Laue fringes (i.e. fringes along q at fixed time) – or equivalently the anti-Bragg oscillations (time dependency of reflectivity at $q_z = 0.19$ Å^{-1}) get damped for increasing film thickness as the growth mode changes from a 2D/layer-by-layer growth of the first monolayers to 3D/mound growth, which is characterized by simultaneous filling of different molecular layers. For growth at 130 °C the anti-Bragg oscillations get damped out after four oscillation maxima (see Fig. 5b top panel), i.e. roughening sets in after ~8 monolayers as one full anti-

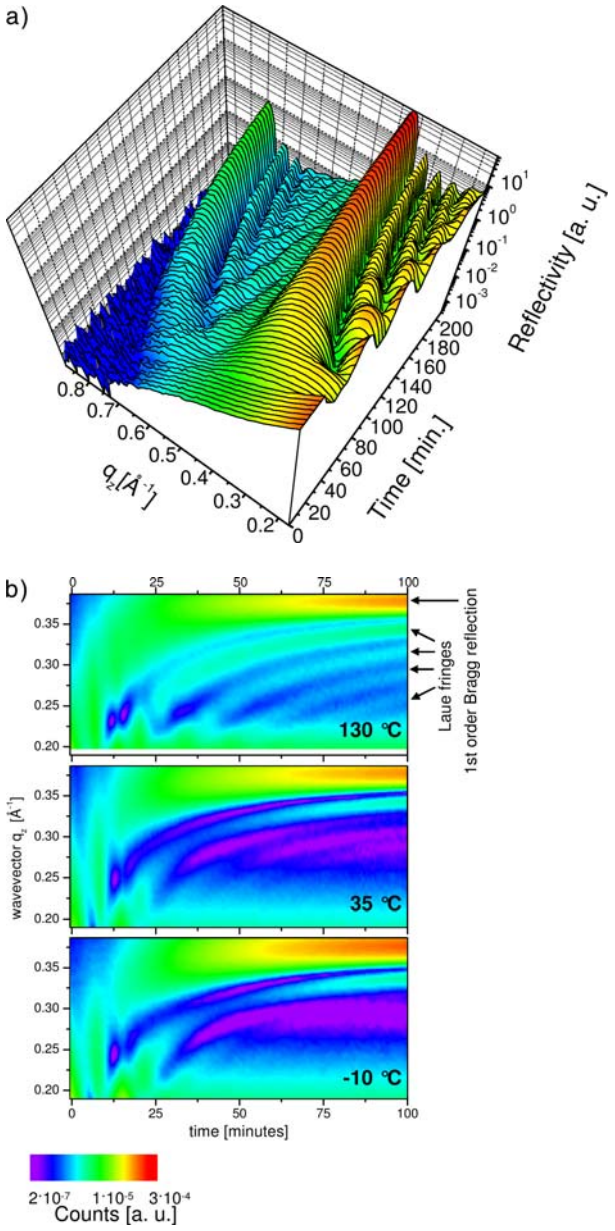

Figure 5 (online colour at: www.pss-a.com) (a) Real-time measurements of the X-ray reflectivity in a wide q-range during DIP deposition on silicon oxide have been performed at beamline ID10B at the ESRF (deposition rate 0.6 Å/min, substrate temperature 130 °C). Two peaks corresponding to the first and second order Bragg reflection of DIP can be seen to grow with increasing deposition time. (b) Reflectivity of DIP thin films grown at 130 °C, 35 °C, and –10 °C substrate temperature with a rate of 3 Å/min on silicon oxide. The datasets comprise a region between the anti-Bragg and the Bragg condition in q, and range from time 0 min (i.e. bare substrate) to 100 min (corresponding to ~240 Å film thickness). In all three measurements a strong Bragg reflection at $q = 0.38$ Å^{-1} develops, showing that a DIP structure with standing upright molecules grows. Next to the Bragg reflections side maxima (Laue-fringes) develop and get narrower with time. At lower substrate temperatures the Laue fringes are damped more strongly indicating that 3D growth (roughening) sets in earlier.

Bragg oscillations corresponds to growth of two monolayers [6]. Compared to pentacene where roughening sets in after four monolayers DIP grows with smooth morphology for twice as long. For subsequent 3D growth, the DIP roughness has been found to increase faster than expected for random deposition of molecules. This rapid roughening has been followed up to film thicknesses of 10^4 Å [44] and has also been found in other organic systems [45]. When lowering the substrate temperatures the DIP anti-Bragg oscillations get damped out, and both for 30 °C and –10 °C the layer-by-layer growth breaks down after only ~2–3 monolayers (Fig. 5b middle and bottom panel). Interestingly, the intensity at the Bragg-reflection is larger for lower growth temperatures, as the roughening leads to mounds with heights greater than the average film thickness, and therefore a larger number of layers scattering in phase. The reasons for the transition from layer-by-layer growth to roughening are not yet well understood for complex organic molecular materials. Strained growth in the first monolayers and strain relaxation may trigger a change in growth mode, but for organic molecules the molecular tilt angle and the molecular conformation may also change during growth. For DIP, it has indeed been found in real-time measurements that the in-plane lattice parameter changes during growth of the first three monolayers, but further work is needed to clarify the connection between growth mode and structural changes.

Apart from the temperature dependent growth dynamics we observe a second structure of 'lying down' molecules (λ-structure) which at lower substrate temperatures competes with the growth of the 'standing upright' (σ-structure). While the λ-structure cannot be seen in the real-time measurements in Fig. 5, GID data show Bragg reflections which correspond to DIP molecules in the 'lying down' phase [6, 70]. This change in molecular orientation does depend on substrate temperature as well as the type of substrate. For growth on silicon oxide at 35 °C, the λ-structure starts to nucleate after a critical thickness of 170 Å, i.e. the lying down structure grows on top of the 'standing upright' structure of DIP (see Fig. 6a). In contrast, when growing DIP on top of the organic semiconductor rubrene no λ-structure nucleates within the thickness range studied. When using A-plane sapphire as a substrate, the nucleation of the lying phase occurs without threshold thickness. The substrate dependent occurence of the λ-structure can be rationalized by regarding the substrate interactions with DIP. Rubrene substrates have only weak van-der-Waals interactions that favour the standing upright structure. In contrast, the stronger effective interaction with sapphire due to the stepped sapphire surface and the slightly higher van-der-Waals interactions lead to molecules adopting a lying down orientation and therefore an early nucleation of the λ-structure. For a more detailed discussion regarding the influence of different substrates and the interaction of the molecules with the substrate see e.g. Ref. [17]. Figure 6b schematically summarizes the connection between substrate interaction and temperature

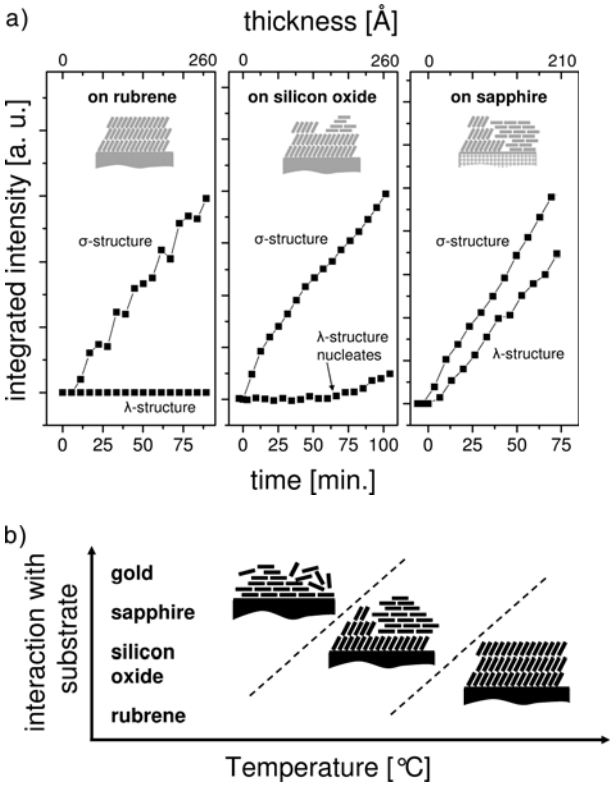

Figure 6 (a) Evolution of the characteristic reflections for the lying down structure (100) and the 'standing upright' structure (11) as a function of time (film thickness), for growth on rubrene (10 °C), silicon oxide, and stepped sapphire (both at 35 °C). Stronger interactions with the substrate promote earlier nucleation of the lying down structure. (b) Schematic showing influence of substrate temperature and strength of interaction with substrate on the orientational transition from lying down to standing upright structures.

with molecular orientation in the thin film. For metal substrates the molecule-substrate interactions are even stronger and as expected the lying down structure has been observed to grow directly on top of polycrystalline gold substrates [71].

4.3 PTCDA on Ag(111), Cu(111), and Au(111)

Perylene-tetracarboxylicacid-dianhydride (PTCDA) is among the most thoroughly studied organic semiconductors [20–22, 72–84], both in the monolayer and multilayer regime.

One of the characteristic features of PTCDA is that it (almost) always grows in a lying-down configuration in contrast to pentacene and DIP, which is probably due to its layered crystal structure and molecular quadrupole moment. A strong interaction of PTCDA with the metal substrates ('chemisorption') is found for Ag(111) [73] and Cu(111) surfaces. Using the XSW technique a bonding distance of $d_0 = 2.86 \pm 0.01$ Å [20, 21] on silver and 2.61 ± 0.02 Å [20] on copper has been measured. A weaker interaction, however, is found for PTCDA on Au(111) with

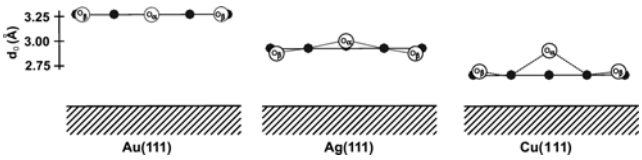

Figure 7 Different bonding distances and adsorption geometries of PTCDA on Au(111), Ag(111) and Cu(111) as measured by XSW [20–22]. From Ref. [28] with permission.

3.27 ± 0.02 Å [22], see Fig. 7. These differences reflect the complex bonding mechanism to the substrates where covalent and the van-der-Waals forces contribute to the interaction. Interestingly, there is a close correlation of these distances with the electronic properties of PTCDA monolayers on the different substrates [28] – an issue which is relevant for the alignment of energy levels at the interface and the charge carrier (electron or hole) injection from the metal contacts into the organic layer. We note that the XSW results of PTCDA/Ag(111) obtained in the monolayer regime agree with surface diffraction data obtained earlier from multilayer films of PTCDA [18]. This indicates that the growth of further layers does not influence the first layer and the XSW measurements of d_0 are indeed relevant beyond the monolayer coverage. Moreover, a substrate dependent distortion of the C = O bonds is found, see Fig. 7: for PTCDA on Ag(111) the carboxylic oxygen atoms are located below the molecular plane ($d_0 = 2.68$ Å), but for PTCDA on Cu(111) these atoms are above the plane ($d_0 = 2.73$ Å). Similar adsorption induced distortions of organic molecules have been observed for NTCDA [23, 24] and F_{16}CuPc [25], respectively.

When grown at low substrate temperatures ($T < 50$ °C at a growth rate of 1 Å/min), PTCDA films exhibit a smooth morphology albeit with poor crystallinity. As is often observed for OMBD, higher substrate temperatures gives improved crystallinity, albeit with a rough morphology with separated crystals on a range of substrates such as PTCDA/InAs(001) [82], PTCDA/NaCl(001), KCl(001) and KBr(001) [81], Au(111) [83, 84], and Ag(111) [74–80]. It turned out that PTCDA exhibits very well-defined Stranski–Krastanov growth on Ag(111) as established in real-time X-ray experiments.

Figure 8 shows anti-Bragg oscillations for PTCDA deposition on Ag(111) at different substrate temperatures clearly demonstrating (1) the decay of crystallinity and therefore growth oscillations at low substrate temperatures, and (2) the damping of oscillations after deposition of two monolayers, indicating a transition from 2D to 3D growth (Stranski–Krastanov growth with two monolayers wetting) [76]. Again fits of the growth oscillations have been performed within the kinematic (single scattering) approximation of X-ray scattering, but in this example kinetic Monte Carlo simulations [86] have been used to model the evolution of the fractional layer coverages $\theta_n(t)$. While temperatures for the calculations systematically lie below the real substrate temperature, indicating that the energy barriers in

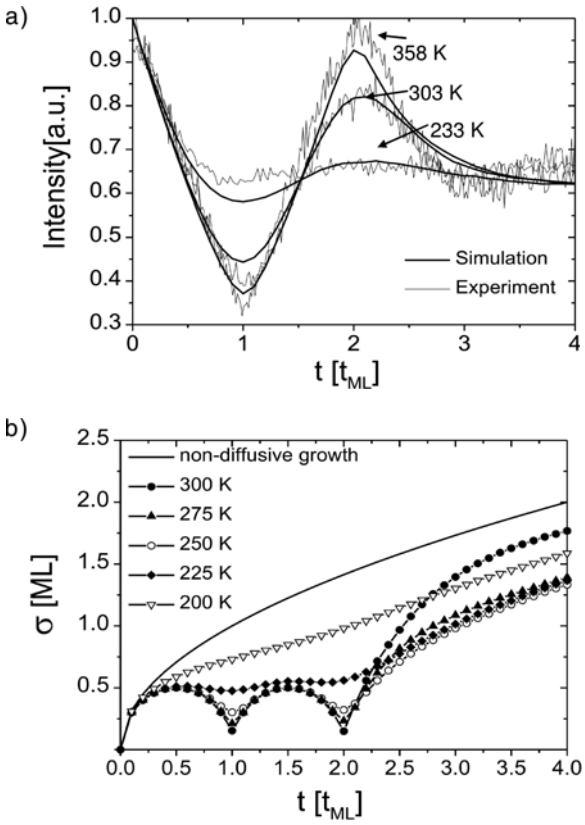

Figure 8 (a) Comparison of experimental anti-Bragg oscillations (substrate temperatures 233 K, 303 K, and 358 K) and Monte Carlo simulations (simulations at 200 K, 225 K, 250 K). (b) Interface roughness σ in units of monolayers (ML) as obtained from Monte Carlo simulations at different temperatures. A clear transition from 2D to 3D growth is visible after two monolayers, which occurs as early as after half a monolayer deposition for low temperatures (200 K). Figures by courtesy of B. Krause and from Ref. [76] with permission.

the calculations are slightly too low, the X-ray growth oscillations are fitted well. This allows a calculation of the film roughness σ from the simulated $\theta_n(t)$ as shown in Fig. 8. At high substrate temperatures the first two layers grow in a well-defined layer-by-layer fashion with a pronounced transition to island growth after two monolayers. The layer-by-layer growth of the first layers is strongly temperature dependent and breaks down for lower substrate temperatures [76].

5 Organic heterostructures Below we discuss selected examples of more complex layer structures, which are essential for organic based devices.

5.1 Metal capping layers Metal contacts are one obvious requirement for many applications of organic semiconductors. It turns out that the controlled deposition of metals on organics, e.g. as 'top electrode', is non-trivial. In order to reduce problems related to interdiffusion (and ultimately short-circuiting) and traps related to surface states, different strategies can be pursued:

– Deposition at low temperatures to 'freeze in' the interdiffusion.

– Deposition at (moderately) high rates with the idea that the metals are quickly forming larger aggregates which are then less mobile and diffuse less far into the organic film.

– Use of 'suitably reactive' metals and/or organics, so that a strong interaction at the top layer(s) of the organic material prevents interdiffusion.

– 'Soft deposition' by 'thermalizing' or at least reducing the energy of the impinging metal atoms by 'baffling' these using a noble gas or other means.

– Miscellaneous other non-thermal deposition strategies including, e.g., electrochemical deposition may be attempted.

We performed studies of the deposition of gold, which is widely used as a hole injection material, onto well-defined DIP thin film surfaces to study the interdiffusion using X-ray reflectivity and transmission electron microscopy (Fig. 9). The study followed the 'classical' approach without specific precaution against interdiffusion except

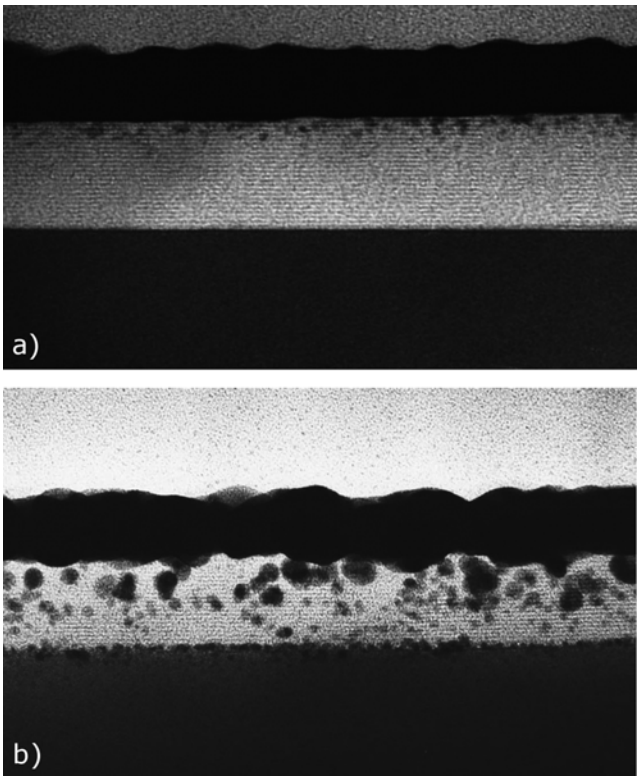

Figure 9 Cross-sectional transmission electron microscopy images of two Au/DIP/silicon oxide hetero-structures. While the Au contact prepared at (a) –120 °C and a rate of 23 Å/min exhibits rather well-defined interfaces, the Au contact prepared at (b) 70 °C and a rate of 0.35 Å/min shows strong interdiffusion. Note that individual lattice planes of the DIP film can be resolved. Figures by courtesy of A. Dürr and from Ref. [86] with permission.

for variation of the temperature and the rate [68, 71, 86–88]. The important result was that under rather typical deposition conditions near room temperature the metal interdiffusion was already significant, and the layers would exhibit electrical shorts, see Fig. 9b. Only if the substrate is cooled, fairly well-defined interfaces could be obtained. Scharnberg et al. [89] found a very similar behaviour for silver capping layers on DIP and pentacene using the complementary approach of radio tracers.

5.2 Insulating capping layers Organic devices eventually have to meet certain stability requirements to preserve their electrical and/or optical characteristics and to guarantee a longterm functioning.

5.2.1 Degradation of devices It is well known that organic semiconductor films exposed to ambient conditions may undergo alterations which significantly affect their optical and electrical properties. For amorphous rubrene films, for example, Käfer et al. [90] could show that exposure to ambient gases leads to the formation of rubreneperoxide at the surface. In Ref. [91] we studied the oxidation and photo-oxidation of rubrene films and found it to be accompanied by a significant change of the optical properties. Other studies focused on the degradation processes of OLEDs and different sources could be identified (see also Ref. [92]) as for example: (1) structural changes of the organic films, i.e. crystallisation of initially amorphous films [93, 94], (2) oxidation/degradation of the top electrodes [95], and (3) gas evolution [96].

A number of recent articles also describe the influence of moisture and ambient gases on device characteristics of organic field-effect transistors (OFETs) [97, 98]. Pannemann et al. [99], for instance, studied the longterm effects of different gases such as oxygen and nitrogen on the performance of OFETs based on pentacene films. During a period of nine months they found a significant decrease in the maximum on-current from initially $-60.9\,\mu A$ to -187 nA while the charge carrier mobility decreased from $2.0 \times 10^{-3}\,cm^2/Vs$ to $1.2 \times 10^{-5}\,cm^2/Vs$. To preserve device characteristics it is obvious that either molecules have to be used which are stable against moisture and oxygen [100] or the devices have to be encapsulated [101]. In this section we will discuss some of our results in the context of recent progress in encapsulating organic devices. Our results focus on the preparation, growth and thermal stability of organic semiconductor films of DIP capped by sputtered aluminium oxide films.

5.2.2 Encapsulation of devices An encapsulation film for organic devices primarily has to fulfil the following requirements:

– protection of organic film and contacts against moisture or ambient gases,

– formation of well-defined interfaces with the organic film, i.e. no diffusion of the capping material into the organic film,

– stability at elevated temperatures,

– sufficient elasticity to be used on flexible substrates.

Different materials have been used to encapsulate organic devices and it has been shown that they can significantly enhance the lifetime of the devices [101–105]. Beyond protection of devices against ambient gases capping layers can also be attributed supplementary functions. Scharnberg et al. [106], for example, used a Teflon-based electret layer as a second gate and encapsulation material which could also be used to tune the threshold voltage of the device. Riel et al. [107] studied the tunability of the emission characteristics of top-emitting OLEDs by means of a dielectric capping layer. Furthermore, Peumans et al. [108] have shown that capping layers can also be used to effectively suppress substantial surface roughening during post-growth annealing of a blend of organic semiconductors.

5.2.3 Aluminium oxide capping layers Aluminium oxide has been successfully used as encapsulation material either as a pure AlO_x capping layer [109] or in combination with polyacrylate as a multilayer coating [110] for OLEDs. Ferrari et al. [111] have studied the effect of a capping layer of aluminium oxide on the electrical properties of thin film transistors (TFT) based on poly-3 hexylthiophene (P3HT). They could show that a P3HT-transitor capped with an Al_2O_3/PVP (poly-vinyl alcohol) layer resulted in almost the same charge carrier mobility as the uncapped transistor. While the uncapped TFT showed a high doping through moisture and oxygen adsorption resulting in an intolerable low on/off ratio the capped transistor was mostly unchanged upon exposure to air.

We prepared aluminium oxide films by radio frequency (r.f.) magnetron sputtering from an aluminium oxide target in a dedicated vacuum chamber. To study the growth and structure of these films deposited on silicon oxide and films of DIP we used X-ray reflectivity, cross-sectional transmission electron microscopy (TEM) and atomic force microscopy (AFM) in contact mode. For further details on the preparation of the aluminium oxide films we refer to Refs. [112, 113].

5.2.3.1 Structure and morphology of aluminium oxide capped DIP films The aluminium oxide films are totally amorphous and consist of small grains. Using cross-sectional TEM, see Fig. 10, we could show that the interface of the aluminium oxide and the DIP film is very well-defined and no significant penetration of aluminium oxide into the organic film could be observed. Furthermore, even individual layers corresponding to the length of upright standing DIP molecules could be observed indicating the high crystallinity of these organic semiconductor films.

Figure 11 shows typical atomic force microscopy (AFM) images (contact mode) of a crystalline DIP film of about 360 Å thickness deposited on silicon oxide (a), an aluminium oxide film (~174 Å thick) deposited on silicon

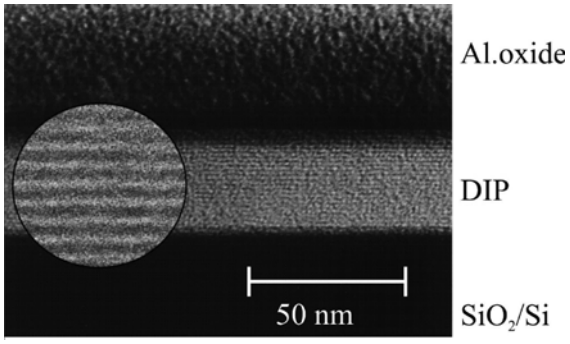

Figure 10 TEM image showing a well-defined heterostructure of aluminium oxide on DIP on silicon oxide together with the monolayered structure of the organic film (inset). With permission from Ref. [114].

oxide (b), and an aluminium oxide film (681 Å) deposited on top of a DIP film (317 Å) (c). After capping DIP films with aluminium oxide the typical graininess of the aluminium oxide morphology on silicon oxide (see Fig. 11b) can be recognised together with the typical DIP topography consisting of large flat terraces of monomolecular step height (upright standing molecules) as shown in Fig. 11a.

5.2.3.2 Growth of aluminium oxide films on silicon oxide and films of DIP As was pointed out in Section 3.2 important information on the growth of thin films can be extracted from scaling theories and it was mentioned that the film roughness σ scales with film thickness D according to $\sigma \sim D^{\beta}$. From the growth exponent β information on the different growth processes involved can be extracted.

Thus, from measuring the aluminium oxide roughness for different film thicknesses the growth exponent β can

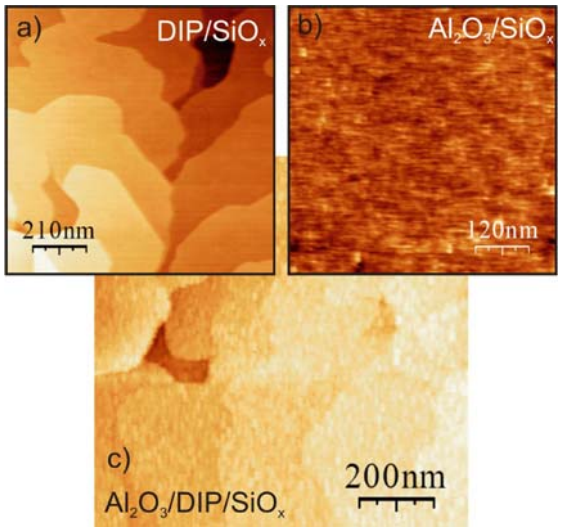

Figure 11 (online colour at: www.pss-a.com) Topographical AFM images (contact mode) of (a) 360 Å DIP on silicon oxide, (b) 174 Å aluminium oxide on silicon oxide, and (c) 681 Å aluminium oxide on a DIP film. With permission from Ref. [112].

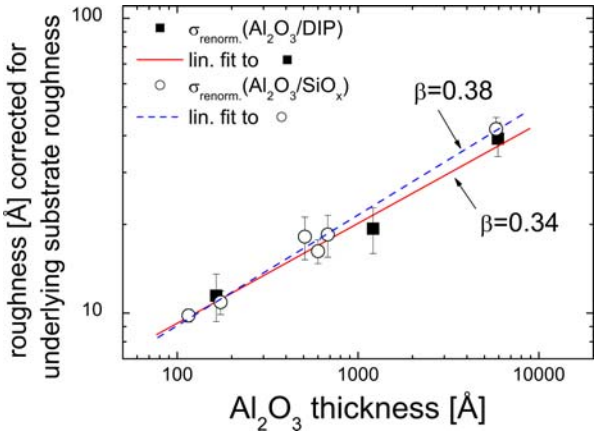

Figure 12 (online colour at: www.pss-a.com) Renormalised roughness $\sigma_{Al_2O_3}^{renorm.}$(DIP) for Al_2O_3/DIP (filled squares) compared to the roughness $\sigma_{Al_2O_3}^{renorm.}$($SiO_x$) of the Al_2O_3/SiO_x system (open circles). The scaling behaviour of aluminium oxide layers deposited on DIP and on SiO_x are in good agreement. With permission from Ref. [112].

by determined as the slope of a linear fit to a log–log plot of the aluminium oxide roughness versus its film thickness. To account for the roughness of the underlying substrate we used a renormalisation according to the relation [10]

$$\sigma_{Al_2O_3}^{renom.} = \sqrt{\sigma_{Al_2O_3}^2 - \sigma_{substr.}^2}$$

with $\sigma_{substr.} = 4$ Å as derived from measurements of the clean substrate.

We have prepared aluminium oxide films on silicon oxide as well as on crystalline films of DIP with thicknesses ranging from 116 Å to ~6000 Å. From the analysis of X-ray reflectivity measurements on these samples we could determine the aluminium oxide surface roughness for different film thicknesses. In Fig. 12 the renormalised aluminium oxide roughness is plotted as a function of its film thickness. For Al_2O_3/SiO_x we could extract a growth exponent of $\beta = 0.38$ and for Al_2O_3/DIP $\beta = 0.34$ [112]. It is quite surprising to find similar growth exponents considering the different chemical nature of the substrates especially the significantly lower surface energy of DIP compared to silicon oxide.

5.2.4 Thermal stability of capped organic films Besides the obvious performance requirements, the devices also have to meet stability standards, which in some cases are actually the limiting factor of technological progress [2]. Indeed, stability at elevated temperatures, high electrical-field gradients, and against exposure to corrosive gases like oxygen is crucial for many commercial applications. Recently, it has been shown that thermal degradation of OLEDs is a serious problem for the lifetime of these devices [115].

To address this problem we have prepared highly crystalline films of the organic semiconductor DIP and capped them with r.f. magnetron sputtered aluminium oxide films.

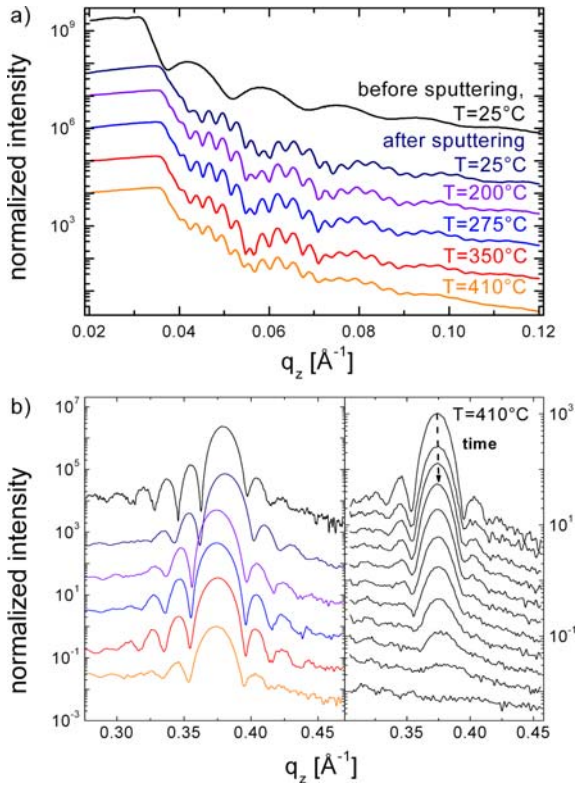

Figure 13 (online colour at: www.pss-a.com) X-ray reflectivity data of the aluminium oxide/DIP multilayer with least-square fits at different temperatures. (a) By heating the sample the initially well-defined Kiessig fringes slowly degrade and the roughness of the DIP/aluminium oxide and aluminium oxide/vacuum interfaces increases with higher temperatures. (b) The first order Bragg peak with Laue oscillations remains visible up to $T = 460$ °C. For clarity the datasets are plotted with an offset. With permission from Ref. [113].

We then performed *in-situ* X-ray reflectivity and grazing incidence diffraction (GID) measurements to study the thermal stability of these samples. Figure 13 shows the reflectivity (a) with the first order DIP Bragg peak (b) for different temperature steps.

Surprisingly, the aluminium oxide/DIP multilayer structure did not show significant changes when heating the sample up to 350 °C. And only around 410 °C, i.e. 210 K above the desorption temperature of uncapped DIP films (on SiO_x) the multilayer structure broke down.

We further investigated the parameters influencing this strong enhancement of the thermal stability and we found that the 'breakdown' temperature depends on the heating rate (heating at lower rate leads to higher breakdown temperatures), the stoichiometry of the aluminium oxide capping layer (aluminium oxide films with higher metallic content were less effective in stabilising the DIP film), and the thickness of the capping layer [113]. The results are summarised in Fig. 14 which shows the integrated intensity of the first order DIP Bragg reflection as a function of temperature. The integrated intensity being proportional to

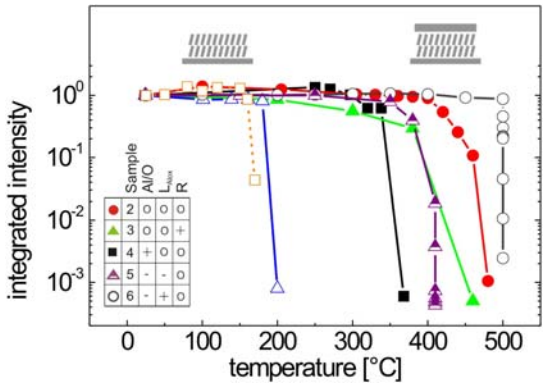

Figure 14 (online colour at: www.pss-a.com) Comparison of the integrated Bragg intensity of different samples. Sample 1 (open triangle) had no capping layer, whereas samples 2–6 had an aluminium oxide capping layer. Variations of the Al/O stoichiometry, the capping layer thickness L_{Alox} and heating rate R (in comparison with sample 2 the symbols –, ○, and + in the inset indicating respectively smaller, similar, and higher values for the particular parameter) result in different breakdown temperatures. Sample 7 (open square) had a gold film instead of an aluminium oxide layer on top of DIP [86]. With permission from Ref. [113].

the number of ordered DIP molecules in the film thus represents the degree of order/crystallinity of the organic film.

From *in-situ* GID measurements we could extract the in-plane DIP unit cell parameters as a function of temperature and found that the thermal expansion of these lattice parameters shows a complex/non-linear behaviour. This suggests that due to the large difference in the thermal expansion of aluminium oxide (6.5×10^{-6} K^{-1} [116]) and the in-plane lattice parameters of uncapped DIP (about an order of magnitude larger) thermal stresses eventually lead to the formation of cracks in the aluminium oxide capping layer which in turn allow for the desorption of DIP molecules through theses defects. This could also be confirmed by thermal desorption spectroscopy measurements. Furthermore, on a long term scale the crystallinity of DIP films was observed to slowly decrease possibly due to defects in the capping layer and consecutive desorption.

Figure 15a shows an optical micrograph of a capped DIP film after a thermal cycle. The DIP film was only deposited in the middle of the silicon oxide substrate and the whole sample was encapsulated with aluminium oxide to prevent desorption of the organic film from the sides. Clearly, a network of cracks formed on the part of the sample where DIP was below the aluminium oxide layer while the capping layer seems unaffected where it covers the silicon oxide. A possible scenario of this breakdown is illustrated in Fig. 15b. Due to mostly thermally induced cracks in the aluminium oxide capping layer DIP is desorbing through the capping barrier. This leads to a decrease in the crystallinity of the organic film as a function of temperature and time. A second possibility for the development of defects in the capping layer is due to Argon inclusions which at elevated temperatures might lead to defects in the encapsulation.

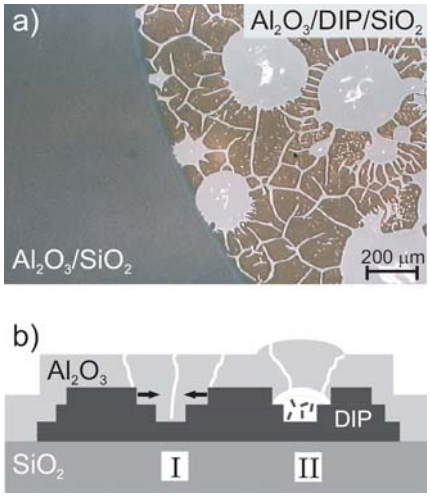

Figure 15 (online colour at: www.pss-a.com) Optical micrograph of a heated Al_2O_3/DIP/SiO_x sample where the DIP film was only deposited in the middle of the sample. An extended network of cracks can be observed which is only limited to regions where the organic film was located underneath. With permission from Ref. [113].

In conclusion, we could show that the thermal stability of crystalline films of DIP can be strongly enhanced by aluminium oxide encapsulation [113, 114]. The important finding is that the crystallinity of these films could be preserved to temperatures up to 300 K above the desorption temperature of uncapped films.

The evidence of the enhanced thermal stability is of great practical importance and it offers a route for the stabilisation of compounds with sapor pressures so far considered too high for utilisation in organic-based devices. Capping layers also allow to measure for example the charge carrier mobility in organic TFTs at temperatures otherwise inaccessible. Meyer et al. [117] have built organic pentacene based TFTs capped with aluminium oxide films and poly-para-xylylene (PPX) and they could measure field-effect for transistors with both capping layers up to temperatures between 140–170 °C, i.e. 50 K above the desorption temperature of pentacene/SiO_x.

6 Conclusion In this review we presented a selection of recent studies on organic thin films and organic-inorganic interfaces which demonstrate that X-ray scattering techniques can be used to investigate the various structural properties as well as the particular growth behaviour of organic molecules. The case studies of pentacene, DIP, and PTCDA deposition show how real-time experiments can be employed to derive detailed information about materials which are relevant for organic device application such as OFETs.

Acknowledgements We wish to thank the DFG for financial support. We would also like to acknowledge numerous fruitful interactions within the DFG focus program 1121 on organic field effect transistors.

References

[1] W. E. Brütting (ed.), Physics of Organic Semiconductors (Wiley-VCH, Weinheim, 2005).
[2] R. Farchioni and G. Grosso, Organic Electronic Materials (Springer, Berlin, 2001).
[3] G. Horowitz, D. Fichou, X. Peng, Z. Xu, and F. Garnier, Solid State Commun. **72**, 381 (1989).
[4] C. D. Dimitrakopoulos and P. R. L. Malenfant, Adv. Mater. **14**, 99 (2002).
[5] D. J. Gundlach, Y. Y. Lin, T. N. Jackson, S. F. Nelson, and D. G. Schlom, IEEE Electron Device Lett. **18**, 87 (1997).
[6] S. Kowarik, A. Gerlach, S. Sellner, F. Schreiber, L. Cavalcanti, and O. Konovalov, Phys. Rev. Lett. **96**, 125504 (2006).
[7] D. Käfer, L. Ruppel, G. Witte, and C. Wöll, Phys. Rev. Lett. **95**, 166602 (2005).
[8] M. Tolan, X-Ray Scattering from Soft-Matter Thin Films (Springer, Heidelberg, 1999).
[9] L. G. Parratt, Phys. Rev. **95**, 359 (1954).
[10] V. Holý, U. Pietsch, and T. Baumbach, High-Resolution X-Ray Scattering from Thin Films and Multilayers (Springer, Berlin, 1999).
[11] H. Dosch, Critical Phenomena at Surfaces and Interfaces, Springer Tracts in Modern Physics, Vol. 126 (Springer, Heidelberg, 1999).
[12] J. Krug and T. Michely, Islands, Mounds and Atoms: Patterns and Processes in Crystal Growth Far From Equilibrium (Springer, Berlin, 2004).
[13] A. Pimpinelli and J. Villain, Physics of Crystal Growth (Cambridge University Press, Cambridge, 1998).
[14] I. V. Markov, Crystal Growth for Beginners: Fundamentals of Nucleation, Crystal Growth and Epitaxy (World Scientific, Singapore, 1994).
[15] A. L. Barabási and H. E. Stanley, Fractal Concepts in Surface Growth (Cambridge University Press, Cambridge, 1995).
[16] F. Schreiber, phys. stat. sol. (a) **201**(6), 1037 (2004).
[17] G. Witte and C. Wöll, J. Mater. Res. **19**, 1889 (2004).
[18] B. Krause, A. C. Dürr, F. Schreiber, H. Dosch, and O. H. Seeck, J. Chem. Phys. **119**, 3429 (2003).
[19] J. Zegenhagen, Surf. Sci. Rep. **18**, 199 (1993).
[20] A. Hauschild, K. Karki, B. C. C. Cowie, M. Rohlfing, F. S. Tautz, and M. Sokolowski, Phys. Rev. Lett. **94**, 36106 (2005).
[21] A. Gerlach, S. Sellner, F. Schreiber, N. Koch, and J. Zegenhagen, Phys. Rev. B **75**, 045401 (2007).
[22] S. K. M. Henze, O. Bauer, T. L. Lee, M. Sokolowski, and F. S. Tautz, Surf. Sci. **601**, 1566 (2007).
[23] J. Stanzel, W. Weigand, L. Kilian, H. L. Meyerheim, C. Kumpf, and E. Umbach, Surf. Sci. Lett. **571**, 311 (2004).
[24] C. Stadler, S. Hansen, A. Schöll, T. L. Lee, J. Zegenhagen, C. Kumpf, and E. Umbach, New J. Phys. **9**, 50 (2007).
[25] A. Gerlach, F. Schreiber, S. Sellner, H. Dosch, I. A. Vartanyants, B. C. C. Cowie, T. L. Lee, and J. Zegenhagen, Phys. Rev. B **71**, 205425 (2005).
[26] C. Stadler, S. Hansen, F. Pollinger, C. Kumpf, E. Umbach, T. L. Lee, and J. Zegenhagen, Phys. Rev. B **74**, 035404 (2006).

[27] R. Woolley, C. Martin, G. Miller, V. Dhanak, and P. Moriarty, Surf. Sci. **601**, 1231 (2007).
[28] S. Duhm, A. Gerlach, I. Salzmann, B. Bröcker, R. L. Johnson, F. Schreiber, and N. Koch, Org. Electron. **9**, 11 (2008).
[29] S. C. B. Mannsfeld and T. Fritz, Mod. Phys. Lett. B **20**, 585 (2006).
[30] A. Hoshino, S. Isoda, and T. Kobayashi, J. Cryst. Growth **115**, 826 (1991).
[31] D. E. Hooks, T. Fritz, and M. D. Ward, Adv. Mater. **13**, 227 (2001).
[32] F. Schreiber, J. Phys.: Condens. Matter **16**, R881 (2004).
[33] M. C. Gerstenberg, F. Schreiber, T. Y. B. Leung, G. Bracco, S. R. Forrest, and G. Scoles, Phys. Rev. B **61**, 7678 (2000).
[34] F. Schreiber, M. C. Gerstenberg, H. Dosch, and G. Scoles, Langmuir **19**, 10004 (2003).
[35] F. Schreiber, M. C. Gerstenberg, B. Edinger, B. Toperverg, S. R. Forrest, G. Scoles, and H. Dosch, Physica B **283**, 75 (2000).
[36] A. S. Killampalli, T. W. Schroeder, and J. R. Engstrom, Appl. Phys. Lett. **87**, 033110 (2005).
[37] D. Käfer, L. Ruppel, and G. Witte, Phys. Rev. B **75**, 085309 (2007).
[38] R. Ruiz, B. Nickel, N. Koch, L. C. Feldman, R. F. Haglund, A. Kahn, and G. Scoles, Phys. Rev. B **67**, 125406 (2003).
[39] H. Klauk, U. Zschieschang, J. Pflaum, and M. Halik, Nature **445**, 745 (2007).
[40] C. E. Aumann, R. Kariotis, and M. G. Lagally, J. Vac. Sci. Technol. A **7**, 2180 (1989).
[41] J. Krug, Adv. Phys. **46**, 139 (1997).
[42] J. Krug, arXiv cond-mat/0403267 (2004).
[43] R. Ruiz, B. Nickel, N. Koch, L. C. Feldman, J. R. F. Haglund, A. Kahn, F. Family, and G. Scoles, Phys. Rev. Lett. **91**, 136102 (2003).
[44] A. C. Dürr, F. Schreiber, V. K. K. A. Ritley, J. Krug, H. Dosch, and B. Struth, Phys. Rev. Lett. **90**, 16104 (2003).
[45] S. Yim and T. S. Jones, Phys. Rev. B **73**, 161305 (2006).
[46] M. C. Lafouresse, P. J. Heard, and W. Schwarzacher, Phys. Rev. Lett. **98**, 236101 (2007).
[47] S. Kowarik, A. Gerlach, S. Sellner, F. Schreiber, J. Pflaum, L. Cavalcanti, and O. Konovalov, Phys. Chem. Chem. Phys. **8**, 1834 (2006).
[48] N. Karl, Charge carrier mobility in organic crystals, in: Organic Electronic Materials, edited by R. Farchioni and G. Grosso (Springer, Berlin, 2001).
[49] E. Chason, T. M. Mayer, A. Payne, and D. Wu, Appl. Phys. Lett. **60**, 2353 (1992).
[50] S. Kowarik, A. Gerlach, W. Leitenberger, J. Hu, G. Witte, C. Wöll, U. Pietsch, and F. Schreiber, Thin Solid Films **515**, 5606 (2007).
[51] R. Ruiz, A. C. Mayer, G. G. Malliaras, B. Nickel, G. Scoles, A. Kazimirov, H. Kim, R. L. Headrick, and Z. Islam, Appl. Phys. Lett. **85**, 4926 (2004).
[52] R. Ruiz, D. Choudhary, B. Nickel, T. Toccoli, K. C. Chang, A. C. Mayer, P. Clanc, J. M. Blakely, R. L. Headrick, S. Iannotta, and G. G. Malliaras, Chem. Mater. **16**, 4497 (2004).
[53] K. I. H. Yoshida and N. Sato, Appl. Phys. Lett. **90**, 181930 (2007).
[54] S. Schiefer, M. Huth, A. Dobinewski, and B. Nickel, J. Am. Chem. Soc. **129**, 10316 (2007).
[55] S. Pratontep, M. Brinkmann, F. Nuesch, and L. Zuppiroli, Phys. Rev. B **69**, 165201 (2004).
[56] F. J. Meyer zu Heringdorf, M. C. Reuter, and R. M. Tromp, Nature **412**, 517 (2001).
[57] L. Casalis, M. F. Danisman, B. Nickel, G. Bracco, T. Toccoli, S. Iannotta, and G. Scoles, Phys. Rev. Lett. **90**, 206101 (2003).
[58] A. C. Mayer, R. Ruiz, R. L. Headrick, A. Kazimirov, and G. G. Malliaras, Org. Electron. **5**, 257 (2004).
[59] A. C. Mayer, R. Ruiz, H. Zhou, R. L. Headrick, A. Kazimirov, and G. G. Malliaras, Phys. Rev. B **73**, 205307 (2006).
[60] A. C. Mayer, A. Kazimirov, and G. G. Malliaras, Phys. Rev. Lett. **97**, 105503 (2006).
[61] I. P. M. Bouchoms, W. A. Schoonveld, J. Vrijmoeth, and T. M. Klapwijk, Synth. Met. **104**, 175 (1999).
[62] S. Kowarik, A. Gerlach, S. Sellner, M. Skoda, and F. Schreiber, submitted.
[63] A. K. Tripathi and J. Pflaum, Appl. Phys. Lett. **89**, 082103 (2006).
[64] M. Münch, Strukturelle Beeinflussung der elektrischen Transporteigenschaften dünner organischer Schichten, Ph.D. thesis, Universität Stuttgart (2001).
[65] V. Pozdin, A. Papadimiraos, and G. Malliaras, private communication (2007).
[66] H. E. Simmons, United states patent 4681834: optical recording element (1987).
[67] H. Antoniadis and A. J. Bard, United states patent 6004685: LED doped with periflanthene for efficient red emission (1997).
[68] A. C. Dürr, F. Schreiber, M. Kelsch, and H. Dosch, Ultramicroscopy **98**, 51 (2003).
[69] A. C. Dürr, F. Schreiber, M. Münch, N. Karl, B. Krause, V. Kruppa, and H. Dosch, Appl. Phys. Lett. **81**(12), 2276 (2002).
[70] A. C. Dürr, B. Nickel, V. Sharma, U. Täffner, and H. Dosch, Thin Solid Films **503**, 127 (2006).
[71] A. C. Dürr, N. Koch, M. Kelsch, A. Rühm, J. Ghijsen, R. L. Johnson, J. J. Pireaux, J. Schwartz, F. Schreiber, H. Dosch, and A. Kahn, Phys. Rev. B **68**, 115428 (2003).
[72] E. Umbach, Prog. Surf. Sci. **35**, 113 (1991).
[73] Y. Zou, L. Kilian, A. Schöll, T. Schmidt, R. Fink, and E. Umbach, Surf. Sci. **600**, 1240 (2006).
[74] L. Kilian, E. Umbach, and M. Sokolowski, Surf. Sci. **573**, 359 (2004).
[75] B. Krause, A. C. Dürr, F. Schreiber, H. Dosch, and O. H. Seeck, Surf. Sci. **572**, 385 (2004).
[76] B. Krause, F. Schreiber, H. Dosch, A. Pimpinelli, and O. H. Seeck, Europhys. Lett. **65**(3), 372 (2004).
[77] B. Krause, A. C. Dürr, K. Ritley, F. Schreiber, H. Dosch, and D. Smilgies, Phys. Rev. B **66**, 235404 (2002).
[78] B. Krause, A. C. Dürr, K. A. Ritley, F. Schreiber, H. Dosch, and D. Smilgies, Appl. Surf. Sci. **175/176**, 332 (2001).
[79] B. Krause, Growth and Structure of the Organic Molecule PTCDA on Ag(111), Ph.D. thesis, Universität Stuttgart (2002).
[80] M. Eremtchenko, J. Schaefer, and F. S. Tautz, Nature **425**, 602 (2003).
[81] D. Schlettwein, A. Back, B. Schilling, T. Friz, and N. R. Armstrong, Chem. Mater. **10**, 601 (1998).
[82] C. Kendrick and A. Kahn, J. Cryst. Growth **181**, 181 (1997).

[83] L. Kilian, E. Umbach, and M. Sokolowski, Surf. Sci. **600**, 2633 (2006).
[84] P. Fenter, F. Schreiber, L. Zhou, P. Eisenberger, and S. R. Forrest, Phys. Rev. B **56**, 3046 (1997).
[85] S. Tan and P. M. Lam, Phys. Rev. B **60**, 8314 (1999).
[86] A. C. Dürr, F. Schreiber, M. Kelsch, H. D. Carstanjen, and H. Dosch, Adv. Mater. **14**, 961 (2002).
[87] A. C. Dürr, F. Schreiber, H. D. C. M. Kelsch, H. Dosch, and O. H. Seeck, J. Appl. Phys. **93**, 5201 (2003).
[88] N. Koch, A. C. Dürr, J. Ghijsen, R. L. Johnson, J. J. Pireaux, J. Schwartz, F. Schreiber, H. Dosch, and A. Kahn, Thin Solid Films **441**, 145 (2003).
[89] M. Scharnberg, J. Hu, J. Kanzow, K. Rätzke, R. Adelung, F. Faupel, C. Pannemann, U. Hilleringmann, S. Meyer, and J. Pflaum, Appl. Phys. Lett. **86**, 024104 (2005).
[90] D. Käfer and G. Witte, Phys. Chem. Chem. Phys. **7**, 2850 (2005).
[91] M. Kytka, A. Gerlach, F. Schreiber, and J. Kováč, Appl. Phys. Lett. **90**(13), 131911 (2007).
[92] H. Aziz and Z. D. Popovic, Chem. Mater. **16**, 4522 (2004).
[93] H. Aziz, Z. Popovic, S. Xie, A. M. Hor, N. X. Hu, C. Tripp, and G. Xu, Appl. Phys. Lett. **72**(7), 756 (1998).
[94] E. M. Han, L. M. Do, N. Yamamoto, and M. Fujihira, Thin Solid Films **273**, 202 (1996).
[95] L. M. Do, E. M. Han, Y. Niidome, M. Fujihira, T. Kanno, S. Yoshida, A. Maeda, and A. J. Ikushima, J. Appl. Phys. **76**(9), 5118 (1994).
[96] H. Aziz, Z. Popovic, C. P. Tripp, N. X. Hu, A. M. Hor, and G. Xu, Appl. Phys. Lett. **72**(21), 2642 (1998).
[97] S. Hoshino, M. Yoshida, S. Uemura, T. Kodzasa, N. Takada, T. Kamata, and K. Yase, J. Appl. Phys. **95**(9), 5088 (2004).
[98] S. Ogawa, T. Naijo, Y. Kimura, H. Ishii, and M. Niwano, Appl. Phys. Lett. **86**(25), 252104 (2005).
[99] C. Pannemann, T. Diekmann, and U. Hilleringmann, J. Mater. Res. **19**, 1999 (2004).
[100] H. Tian, J. Shi, D. Yan, L. Wang, Y. Geng, and F. Wang, Adv. Mater. **18**, 2149 (2006).
[101] P. E. Burrows, V. Bulovic, S. R. Forrest, L. S. Sapochak, D. M. McCarty, and M. E. Thompson, Appl. Phys. Lett. **65**(23), 2922 (1994).
[102] C. Pannemann, T. Diekmann, and U. Hilleringmann, 5th International Conference on Polymers and Adhesives in Microelectronics and Photonics (2005), p. 63.
[103] J. Lewis and M. Weaver, IEEE J. Sel. Top. Quantum Electron. **10**, 45 (2004).
[104] K. Yamashita, T. Mori, and T. Mizutani, J. Phys. D, Appl. Phys. **34**(5), 740 (2001).
[105] K. Tsukagoshi, I. Yagi, K. Shigeto, K. Yanagisawa, J. Tanabe, and Y. Aoyagi, Appl. Phys. Lett. **87**(18), 183502 (2005).
[106] M. Scharnberg, V. Zaporojtchenko, R. Adelung, F. Faupel, C. Pannemann, T. Diekmann, and U. Hilleringmann, Appl. Phys. Lett. **90**(1), 013501 (2007).
[107] H. Riel, S. Karg, T. Beierlein, W. Riess, and K. Neyts, J. Appl. Phys. **94**(8), 5290 (2003).
[108] P. Peumans, S. Uchida, and S. R. Forrest, Nature **425**, 158 (2003).
[109] S. H. K. Park, J. Oh, C. S. Hwang, J. I. Lee, Y. S. Yang, H. Y. Chu, and K. Y. Kang, ETRI J. **27**, 545 (2005).
[110] A. B. Chwang, M. A. Rothman, S. Y. Mao, R. H. Hewitt, M. S. Weaver, J. A. Silvernail, K. Rajan, M. Hack, J. J. Brown, X. Chu, L. Moro, T. Krajewski, and N. Rutherford, Appl. Phys. Lett. **83**(3), 413 (2003).
[111] S. Ferrari, F. Perissinotti, E. Peron, L. Fumagalli, D. Natali, and M. Sampietro, Org. Electron. **8**, 407 (2007).
[112] S. Sellner, A. Gerlach, S. Kowarik, F. Schreiber, H. Dosch, S. Meyer, J. Pflaum, and G. Ulbricht, Thin Solid Films, **DOI** 10.1016/j.tsf.2007.12.151.
[113] S. Sellner, A. Gerlach, F. Schreiber, M. Kelsch, N. Kasper, H. Dosch, S. Meyer, J. Pflaum, M. Fischer, B. Gompf, and G. Ulbricht, J. Mater. Res. **21**, 455 (2005).
[114] S. Sellner, A. Gerlach, F. Schreiber, M. Kelsch, N. Kasper, H. Dosch, S. Meyer, J. Pflaum, M. Fischer, and B. Gompf, Adv. Mater. **16**, 1750 (2004).
[115] Y. J. Lee, H. Lee, Y. Byun, S. Song, J. E. Kim, D. Eom, W. Cha, S. S. Park, J. Kim, and H. Kim, Thin Solid Films **515**, 5674 (2007).
[116] R. G. Munro, J. Am. Ceram. Soc. **80**, 1919 (1997).
[117] S. Meyer, S. Sellner, F. Schreiber, H. Dosch, G. Ulbricht, M. Fischer, B. Gompf, and J. Pflaum, Mater. Res. Soc. Symp. Proc. **965**, 0965-S06-13 (2007).

